Enhancement of mechanical and durability properties of preplaced lightweight aggregate concrete

Bo Peng [1a], Jiantao Wang [1,2b], Xianzheng Dong [1a], Feihua Yang [3c], Chuming Sheng [1b] and Yunpeng Liu[*1]

[1] *State Key Laboratory of Silicate Materials for Architectures, Wuhan University of Technology, Wuhan, 430070, China*
[2] *Huarun Cement Research & Development Co.Ltd, Guangzhou, 410460, China*
[3] *Beijing Building Materials Academy of Sciences Research, Beijing, 100041, China .*

Abstract. In this study, the effect of two types of aggregates (fly ash aggregate and shale aggregate) on the density, strength, and durability of preplaced lightweight aggregate concrete (PLWAC) was studied. The results showed that the 7 - 28 days strength of concrete prepared with fly ash aggregates (high water absorption rate) significantly increased, which could attribute to the long-term water release of fly ash aggregates by the refined pore structure. In contrast, the strength increase of concrete prepared with shale aggregates (low water absorption rate) is not apparent. Although PLWAC prepared with fly ash aggregates has a lower density and higher strength (56.8 MPa @ 1600 kg/m^3), the chloride diffusion coefficient is relatively high, which could attribute to the diffusion paths established by connected porous aggregates and the negative over-curing effect. Compared to the control group, the partial replacement of fly ash aggregates (30%) with asphalt emulsion (20% solid content) coated aggregates can reduce the chloride diffusion coefficient of concrete by 53.6% while increasing the peak load obtained in a three-point bending test by 107.3%, fracture energy by 30.3% and characteristic length by 103.5%. The improvement in concrete performance could be attributed to the reduction in the water absorption rate of aggregates and increased energy absorption by polymer during crack propagation.

Keywords: durability; lightweight aggregate concrete; mechanical properties; polymer

1. Introduction

Lightweight aggregate concrete (LWAC) has found wide applications in high-rise buildings, long-span bridges, floating platforms, and severe weathering areas due to its advantages, including lightweight, thermal insulation, fire resistance, and good durability (Real *et al.* 2021, Aungatichart *et al.* 2022). Recently, the incorporation of lightweight aggregate concrete in the designs of steel-concrete composites (Chia *et al.* 2014) or flat steel plate-lightweight aggregate concrete hollow composite slab (Al-Azzawi and Shallal 2021, Yang *et al.* 2019) has attracted wide attention. Moreover, the sintered (Chiou and Chen 2011) or cold-bonded artificial lightweight aggregates (Vali Kolimi and Murugan 2020) prepared by solid wastes or the incorporation of waste like cement kiln dust (Shoaei *et al.* 2017) is considered a green technology in LWAC production.

Compared with ordinary concrete (Normal weight concrete, NWC), the strength of LWAC is primarily controlled by the strength of the lightweight aggregate (LWA), which could reach a ceiling strength. The strength of LWAC increases with an increase in density so that while a 20 MPa mix might be achieved for a density of 1200 kg/m^3, this value would increase to 1800 kg/m^3 for an 80 MPa mix (Lilja *et al.* 1998). However, in practical engineering, the compressive strength of LWAC is usually less than 60MPa at a density of less than 1950 kg/m^3. Moreover, the elastic modulus of LWAC is about 25 – 50 % lower than that of NWC. The different properties have also affected the design of the structures. For example, according to ACI 318, an amplification modification factor is usually needed in the required minimum ratio of column depth to maximum beam longitudinal bar diameter during the design of earthquake-resistant structures.

On the other hand, precast concrete, which usually adopts a steam-curing process, has been used to produce masonry blocks and wall panels due to its high production efficiency (Revilla-Cuesta *et al.* 2022). Moreover, incorporating LWA in precast concrete reduces the concrete's weight and shows comparable structural performance to conventional concrete (Coo and Pheeraphan 2016). However, reaching a higher strength with lowered density is a challenging problem (Vakhshouri and Nejadi 2017).

Preplaced aggregate concrete also refers to concrete prepared by the "two-stage casting method" or "Rock-filled concrete" (An *et al.* 2014), defined as concrete produced by placing coarse aggregates firstly in the formwork and then filling the voids between them with cement grouting paste (Najjar *et al.* 2014). Preplaced aggregate concrete has been

---

∗Corresponding author, Ph.D., Vice Professor,
  E-mail: liuyunpeng@whut.edu.cn
[a] Master Student
[b] Ph.D. Student
[c] Ph.D.

widely used in concrete repair, underwater concrete, and hydraulic engineering (Siddique *et al*. 2021).

Preplaced lightweight aggregate concrete (PLWAC) usually has a higher coarse aggregate content which could decrease concrete density. Therefore, several researchers have investigated the mechanical characteristics of PLWAC. For example, Yoon *et al*. (2015) and Du *et al*. (2017) reported low-density concrete 1500 kg/m^3 with 20 MPa and 1800 kg/m^3 with 44 MPa, respectively. Yoon and Kim (2019) also applied a micromechanical four-phase model to predict the elastic moduli of PLWAC and determined the fluidity of injectable grout using ultrasonic tomography (Yoon *et al*. 2020). Moreover, PLWAC showed a high modulus of elasticity and low shrinkage due to the packing of lightweight aggregates (Du *et al*. 2017).

However, more dedicated research needs to be carried out on improving PLWAC properties. On the one hand, the strength of PLWAC needs to be further enhanced at a relatively low density. PLWAC usually cracks through the lightweight aggregate particle (Abdelgader and Elgalhud 2008), which indicates that a stiff and fully connected aggregate skeleton could increase the compressive strength of grouts with the same w/c (Yoon and Kim 2019). How the improvement of lightweight aggregate strength affects concrete strength needs to be studied. On the other hand, the durability of PLWAC has seldom been investigated. For conventional lightweight aggregate concrete, the interfacial transition zone (ITZ) between the lightweight aggregates and cement paste is dense due to the internal curing effect, which provides good durability. The durability of PLWAC with a high volume of lightweight aggregate (varied water rate) needs to be investigated.

In this study, two types of lightweight aggregates (spherical fly ash LWA and gravel shale LWA) with different water absorption rates and crushing strengths were used to prepare PLWAC, and their effect on concrete strength and durability was investigated. Furthermore, asphalt emulsion was used to coat spherical fly ash LWA and is expected to enhance the concrete toughness and durability, as shown in our previous study (Liu *et al*. 2021). The results hopefully shed some light on the lightweight concrete.

2. Experimental investigations

2.1 Materials

Portland cement CEM I 42.5 (type N, short for C), and silica fume (SF) were used to prepare a grouting cement paste. The physical properties of Portland cement are shown in Table 1, and the chemical compositions of cement and silica fume are shown in Table 2. The physical properties of lightweight aggregates (spherical fly ash LWA and gravel shale LWA) are shown in Table 3. The photographs of LWA used are shown in Fig. 1. Fly ash LWA have a high crushing strength (20.35 MPa) and 24 h water absorption rate (16.39 %). Relatively large-sized particles (larger than 5 mm) are

(a) Fly ash aggregates

(b) Shale aggregates

Fig. 1 Photographs of LWA used

Table 1 Physical properties of cement

Setting time (min)		Flexural strength (MPa)		Compressive strength (MPa)		Density (g/cm^3)	Surface area (m^2/kg)
Initial setting	Final setting	7d	28d	7d	28d		
212	282	5.6	8.4	26.1	50.4	3.14	349

Table 2 Chemical compositions of cement and silica fume (wt.%)

	CaO	SiO$_2$	Al$_2$O$_3$	Fe$_2$O$_3$	SO$_3$	MgO	K$_2$O
C*	55.6	26.3	6.2	3.8	2.8	1.9	1.0
SF*	0.9	93.06	-	2.06	1.28	0.7	1.15

*C-Cement; SF-Silica fume

Table 3 Physical properties of LWA

Type	Bulk density (kg/m^3)	Apparent density (kg/m^3)	Crushing strength (MPa)	Shape	24 h water absorption (%)	Particle size (mm)
Shale (S)	920	1667	9.61	Gravel	3.35	5-16
Fly ash (F)	990	1547	20.35	spherical	16.39	5-10

Table 4 Properties of cationic asphalt emulsion

Solid content (%)	Penetration @ 25℃ (mm)	Ductility @15℃ (cm)	Breaking speed
51	96	130	Moderate

recommended to ensure the injectability of the grout (Yoon *et al*. 2019). A cationic asphalt emulsion was used to coat lightweight aggregates, and its physical properties are shown in Table 4.

2.2 Mix design

Both grout and aggregates properties determine the performance of PLWAC. The grout needs a high flow ability, and fine aggregates are not used to fulfill the small voids between the tightly packed aggregates. Table 5 shows the mix proportion of the grout and its fluidity was 28 s (test according to ASTM C939) (ASTM 2016), and compressive strength was 53.7 MPa.

The effect of aggregate types and particle size on the mechanical properties of concretes was investigated. F and S represent the concrete prepared with fly ash aggregate (F) and shale aggregate (S). 5-10, 10-16, and 5-16 represent the particle size of 5-10 mm, 10-16 mm, and 5-16 mm, respectively. The mix proportions of PLWAC are shown in Table 6.

The dried aggregates were soaked in asphalt emulsion and stirred. Then, the asphalt-coated aggregates were filtered out and dry to form asphalt film on the surface of the aggregates.

Three groups were designed as 20-30, 20-100, and 40-30. Of which, 20 and 40 represent the solid content of the asphalt emulsion is 20% and 40%, respectively. 30 and 100 represent the replacement ratio of ordinary aggregates by asphalt-coated aggregates is 30% and 100 %, respectively.

2.3 Mix and casting procedure

Firstly, lightweight aggregates were pre-placed in the steel mold. Then a grout was prepared and poured from the top of the aggregate by gravity, as shown in Fig. 2. The detailed casting procedure of PLWAC is described by Yoon *et al*. (2015).

The steam-curing regime used in this study is shown in

Table 5 Mix proportions of grout and its physical performance

W/B*	Cement (%)	SF (%)	Superplasticizer content (%)	Flow time (s)	Compressive strength (MPa)
0.35	94	6	1	28	53.7

*W/B- Water/Binder ratio

Table 6 Mix proportions of PLWAC (kg/m^3)

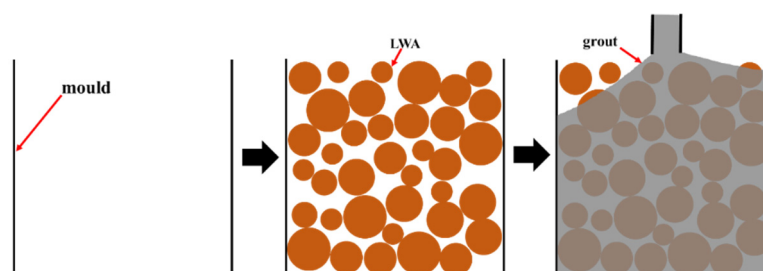| Group	C	SF	LWA*	Water	W/B	Superplasticizer (SP, wt.%)
F (5-10)	529	31	1152	196	0.35	1.0%
S (5-10)	649	39	902	240.8	0.35	1.0%
S (10-16)	667	40	882	247.4	0.35	1.0%
S (5-16)	606	36	950	224.7	0.35	1.0%

*LWA-Lightweight aggregate

Fig. 2 Casting process of PLWAC
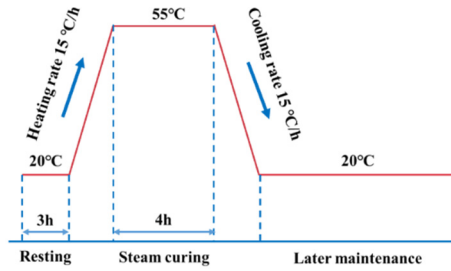
Fig. 3 Steam-curing regime for PLWAC

Fig. 3. After steam-curing, the concrete was subsequently cured under dry curing conditions (20 ± 2°C, RH ≥ 85%) for 28 days (Nie *et al*. 2016).

2.4 Experimental methods

This section mainly introduced the experimental methods to test the aggregates' properties and samples' properties.

(1) Aggregate packing density

The aggregates were first immersed in water for 24 h and then wiped to surface dry before thoroughly packed in a 5 L cylinder mould. Then, the mass of the cylinder mould was weighed as m_1. Subsequently, water was added to fill the cylinder, and the mass of the cylinder was weighed as m_2. Finally, the aggregate packing density, D, was calculated as Eq. (1).

$$D = \frac{m_2 - m_1}{\rho_{H_2O}} \qquad (1)$$

Wherein m_1 and m_2 are the mass of cylinder mould with packing aggregates before and after adding water, respectively; ρ_{H_2O} was the density of water.

(2) Compressive strength test

The compressive strength test was conducted on 100 mm × 100 mm × 100 mm concrete cubes using a 3,000 kN capacity testing machine according to GB 50081-2002. The loading rate was 0.5 MPa/s. Three samples were tested and the average value was calculated. The coefficients of variation is 0.1 MPa.

(3) Dry density of concrete

The dry apparent density of LWAC was tested according to JGJT 12-2019. Three concrete specimens of 100 mm × 100 mm × 100 mm were placed in the oven at 105 - 110°C, dried to constant weight, and weighed to obtain their mass. The sample's length, width, and height were taken as the average of the four corresponding sides measured by vernier calipers to calculate the volume of the specimen. The dry apparent density of concrete was obtained by dividing the mass by the volume. The average value of three specimens was taken as the test result, which is accurate to 1 kg/m³.

(4) Rapid chloride migration (RCM) test

In this paper, the rapid chloride migration test (RCM) was conducted regarding the GB/T 50082 - 2009, which is similar to NordTest NTBuild 492. The molded specimens were cylinders with a diameter of 100 mm and a height of 200 mm, which were cut into cylinders with a diameter of 100 mm and height of 50 mm before testing for 7 days and then continued to be cured until the corresponding age. Each group of tests included 3 specimens.

The specimens were kept in saturated calcium hydroxide solution for 24 hours before testing. The specimens were wrapped in silicone sleeves and tightened with stainless steel hoops. The specimens' bottom and top were submerged in 10 wt% NaCl solution and 0.3 mol/L NaOH solution, respectively. Then the samples were subjected to voltage through the cathode and anode plates. The direct current voltage of 30 V was applied initially, and the test voltage and time were determined according to the initial current. After testing, the specimen was taken out and cleaned, then split into two halves using a press, then spraying $AgNO_3$ solution with a concentration of 0.1 mol/L immediately for color displaying. After 15 min, the white part of the specimen was measured as the depth of the chlorine-ion infiltration area.

The following equation (Eq. (2)) can calculate the unsteady state chloride migration coefficient Dnssm of concrete.

$$D_{nssm} = \frac{0.0239 \times (273 + T)L}{(U-2)t} \left(x_d - 0.0238 \sqrt{\frac{((273+T)L_{x_d})}{U-2}} \right) \qquad (2)$$

Where Dnssm is the unsteady state chloride ion migration coefficient of concrete ($\times 10^{-12}$ m²/s), U is the applied voltage (V), T is the average of the initial and ending temperatures of the anodic sodium hydroxide solution (°C), L is the thickness of the specimen, x_d is the average depth of penetration of chloride ions (mm), and t is the test duration (h).

(5) Water absorption

The water absorption test was performed according to ASTM C 1585-13. Three samples with dimensions of φ100 mm × 50 mm were tested. The initial and secondary rates of water absorption (mm/s$^{1/2}$) are defined as the slope of the line by the least squares regression for the plot of i against the square root of time (s$^{1/2}$) corresponding to all the points from 30 s to 24 h and 1 d to 9 days, respectively.

(6) Mercury intrusion porosimetry (MIP) test

Cement stones around the aggregate were removed from the concrete as test samples and preserved in isopropyl alcohol to stop hydration. At a selected curing age, the samples were dried in a vacuum drying oven at 55°C to constant weight. An AutoPore IV 9500 high-performance automated mercury piezometric tester was used to perform the mercury piezometric test, with a test sample size of 5 - 6 mm and a weight of 3 g.

(7) Hydration degree

The hydration degree test was performed according to the chemically combined water method. First, the hardened cement pastes were crushed and passed through an 80 μm sieve. Next, the specimens were placed in the crucible with a lid sintered at 1,050°C and dried at 105°C for 24 h. The mass was weighed as m1. Then the sealed crucible was

placed in a high-temperature furnace to 1,050°C for three hours to remove all the chemically bound water and cooled to 105°C. Subsequently, it was cooled to room temperature and weighed as m_2. Then the samples were taken out, and the mass of the empty crucible was weighed as m_3. The chemically bound water content of 1 g of fully hydrated cement is 0.25 g. Therefore, the hydration degree of samples can be calculated by Eq. (3).

$$HD = \frac{m_1 - m_2}{(m_2 - m_3) \times 0.23} \times 100\% \quad (3)$$

Wherein HD is the hydration degree of cement; m_1 is the total mass of the crucible and the sample after drying (g); m_2-the total mass of the crucible and sample after burning (g); m_3-the mass of the empty crucible after burning (g).

(8) Asphalt film thickness on the aggregate surface

The asphalt film thickness on the surface of the aggregates was measured under a stereomicroscope. Each group of specimens was measured six times, and the average thickness was calculated.

(9) Three-point bending tests

Three-point bending tests were performed with an electro-hydraulic servo press in displacement control mode with a loading rate of 0.02 mm/min (Gao *et al.* 2022). The crack mouth opening displacement (CMOD) and the mid-span deformation of concrete samples were obtained during three-point bending. The fracture energy G_f of concrete can be calculated according to Eq. (4).

$$G_F = \frac{W_0 + mg\delta_{max}}{(h - a_0)t} \quad (4)$$

Wherein W_0 is the work done by the external load along the direction of the load in the span, i.e., the area enclosed by the load-deflection curve and the transverse coordinate (N/m); m_g is the weight of the beam (N); h is the height of the sample; a_0 is the length of the precast crack; t is the thickness of the specimen; δmax is the maximum deflection value in the middle of the span (m).

The characteristic length L_{ch} was calculated as Eq. (5) to evaluate the brittleness of concrete, and a higher value indicates less brittleness of the concrete (Hillerborg *et al.* 1976).

$$L_{ch} = \frac{EG_F}{f_t^2} \quad (5)$$

Wherein L_{ch} is characteristic length; E is elastic modulus (GPa); f_t is tensile strength (MPa); G_f is fracture energy (N/m).

3. Results and discussion

3.1 Effect of aggregates types on the mechanical properties

Fig. 4 shows the effect of aggregate particle size on aggregate compactness. F5-10 has the tightest aggregate packing volume of 61.6% because spherical aggregates were easier to compact than gravel aggregates due to the ball effect and smooth surface. For shale aggregates, S5-16 has the highest packing density of 58.67%, while S5-10 and S10-16 show packing volumes of 55.73% and 54.45%, respectively. With a continuous particle size (5-16 mm), the voids between the large aggregates could be filled with smaller aggregates, increasing the aggregates' compactness. While for intermittent gradation (5-10 mm and 10-16 mm), the aggregates with larger particle sizes would show more voids, decreasing the compactness.

The apparent dry density (Harden density) and compressive strength of the concretes are shown in Fig. 5. F 5-10 has a minimum apparent density of 1606 kg/m³, while the apparent dry density of S5-10, S10-16, and S5-16 is1633, 1670, and 1615 kg/m³, respectively. Generally, the volume fraction of LWA directly determines the concrete density due to the low density of LWA. Therefore, the LWC density positively correlates with the volume fraction of lightweight aggregates shown in Fig. 4.

As for the compressive strength results, F5-10 showed the highest 28 days strength of 56.8 MPa. While for the concrete prepared with shale aggregates, the 28 days strength of S5-10, S10-16, and S5-16 are 41.0, 39.9, and 46.8 MPa, respectively. For the same aggregate type (shale aggregate), the strength result is correlated with the aggregate compactness of the concrete. That is, the concrete with higher compactness showed a higher compressive strength.
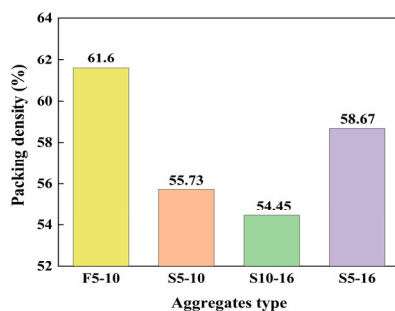

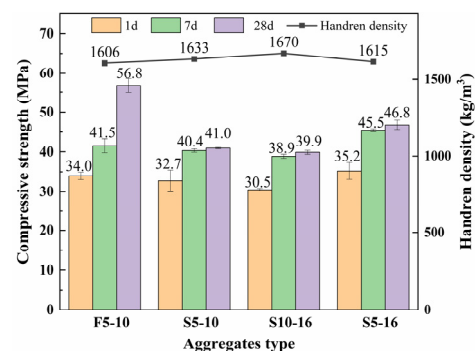Fig. 4 Packing density of different aggregates and particle size

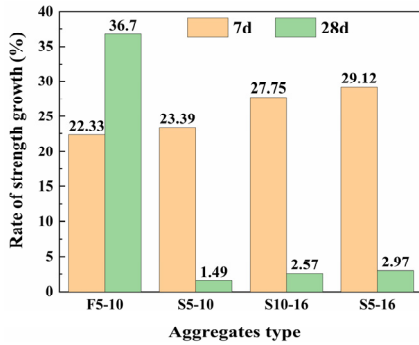Fig. 5 Effect of aggregate type on concrete strength and density

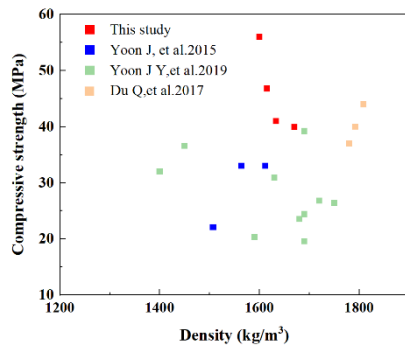Fig. 6 Strength growth rate of concretes at different ages

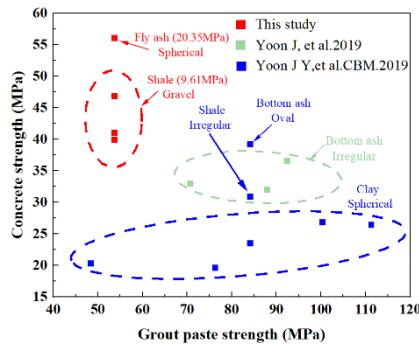Fig. 7 Relation between density and concrete strength

Fig. 8 Relation between mortar strength and concrete strength

However, it is worth noting that with the same particle size distribution (5-10 mm), the 1d and 7d strengths of F5-10 are similar to that of S5-10. Fig. 6 shows the strength growth rate at different curing ages (1-7 days and 7-28 days strength). The strength increase rate of shale aggregate concrete is higher than that of fly ash aggregate concrete from 1-7 days. However, the strength increase rate of 7-28 days (F5 -10) is 36.7%, significantly higher than that of the other three groups (S 5-10, S 10-16, and S 5-16, about 1.5-3.0 %).

From the above experiments, two preliminary conclusions could be drawn: a. In the early 1 and 7 days, the strength of F5-10 is similar to that of shale aggregate concrete. However, in 7-28 days, F5-10 concrete has a significant strength growth rate, showing the highest 28d strength. Considering that the crushing strength of fly ash aggregate (about 20 MPa) is about twice that of shale aggregates (about 10 MPa), the prepared concrete with fly ash aggregate is expected to show a higher strength. The similar early strength (1 day and 7 days) between the fly ash aggregate concrete and shale aggregate concrete may be attributed to the following reasons. On the one hand, gravel shale aggregates play a better interlock effect than spherical fly ash aggregate, which benefits the concrete strength. On the other hand, the strength of the grout may be the ceiling strength for the prepared concretes.

Fig. 7 compares the data obtained in this study and those obtained from other references that carried PLWAC research. What needs to be noted is that the samples used oven-dried lightweight coarse aggregates and did not use any fine aggregates to ensure the grouting performance. The aggregates used in the references and their crushing strength are summarized in Fig. 8. The PLWAC prepared in this study showed a relatively high strength and a low density. Fig. 8 lists the strength of the prepared concrete and the grouting paste. For the same aggregates (clay spherical aggregate), when the grout strength increases from 48 to 111 MPa, the concrete strength slightly increases from 20 to 26 MPa. While for the grout with a fixed w/c ratio (85 MPa), the change in aggregate types (clay, shale, and bottom ash) leads to a different concrete strength (22.5, 31.5, and 40 MPa). It can be speculated that the crushing strength of aggregates somehow limits the PLWAC strength, similar to the ceiling strength of conventional
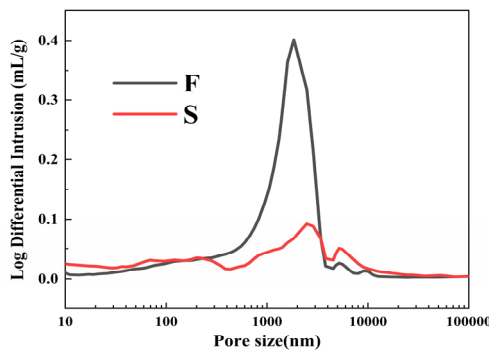
(a) Pore size distribution
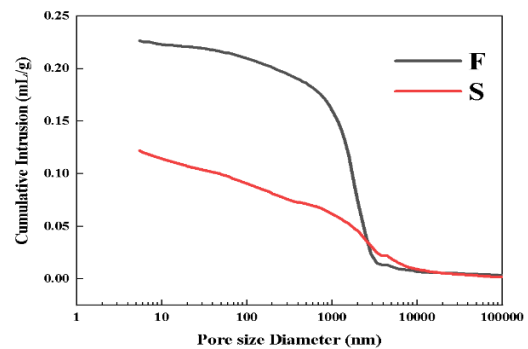
(b) Cumulative pore size distribution

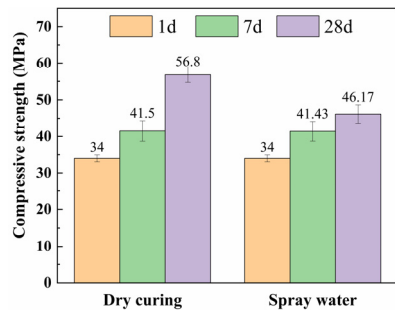Fig. 9 Pore structure of two aggregates by MIP test

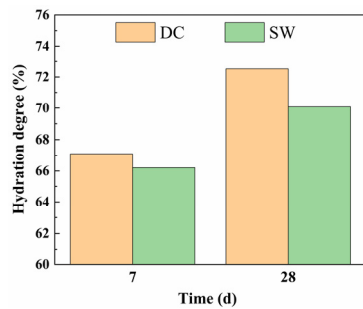Fig. 10 Effect of curing method on F5-10 strength

Fig. 11 Hydration degree of cement paste around aggregates

Table 7 Chloride diffusion coefficient of different concretes

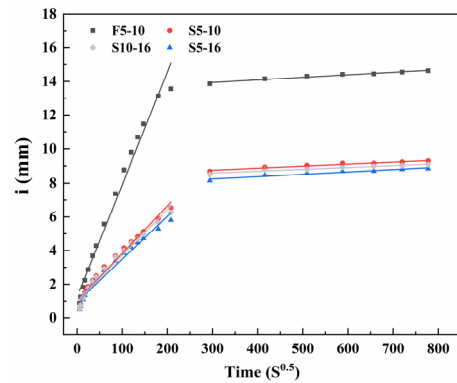| Group	Chloride diffusion coefficient($\times 10^{-12}$m^2/s)
F5-10	21.85
S5-10	9.58
S10-16	7.24
S5-16	6.50

Fig. 12 Capillary water absorption rate of different concretes

Table 8 Initial (S_1) and secondary (S_2) water absorption coefficient of concretes

	F5-10	S5-10	S10-16	S5-16
S_1/(mm·S$^{-0.5}$)	0.0665	0.0282	0.0255	0.0273
S_2/(mm·S$^{-0.5}$)	0.0015	0.0011	0.0011	0.0013
R^2(S1)	0.9813	0.9755	0.9655	0.9719
R^2(S2)	0.9602	0.9472	0.9175	0.9168

lightweight concrete limited by aggregate strength (Haller *et al*. 2023).

The remarkable difference in the strength growth rate in the early stage (1-7 days) and late period (7-28 days) can be explained by the water release and curing effect of different LWAs. Nie *et al*. (2016, 2018) found that during the steam curing process, the water release rate V(r) of LWA is proportional to the pore radius of aggregates. Fig. 9 shows the MIP porosity results of two aggregates. The porosity of fly ash aggregates is mainly within 10 μm, which is smaller than that of shale aggregates. So, the fly ash aggregates showed a slower water release rate, providing an internal curing effect during late age (7-28 days). In contrast, the amount of water released by shale aggregates in the early stage (7 days) is large, showing a marginal curing effect in the late age.

To further verify this speculation, the effect of dry curing and spray water curing (20 ± 2℃, RH ≥ 95%) on the strength of F5-10 was shown in Fig. 10. At the initial seven days, the curing method has a marginal impact on the strength. However, when the curing age increased to 28 days, the concretes with drying curing showed an increased strength by about 19 % compared to the concrete with spray water curing. Fig. 11 shows the effect of curing methods on the hydration degree of the cement pastes around the aggregate. For dry curing, the hydration degree increased from 67% of 7 days to 73% of 28 days. While that of cement pastes cured with spray water increased from 66% of 7 days to 70% of 28 days. This indicated that dry curing benefits the water release of fly ash aggregates and improves the hydration degree.

3.2 Effect of aggregates types on the durability of PLWAC

Table 7 shows the effect of aggregate type on the chloride diffusion coefficient of PLWAC. For shale aggregate concrete, the diffusion coefficient positively correlated with the volume fraction of the LWA. Though F5-10 concrete has the highest 28 days strength, its chloride diffusion coefficient is significantly higher than that of concrete prepared with shale aggregate. Fig. 12 shows different concretes' capillary water absorption results, and Table 8 summarizes the fitted capillary water absorption rate. Similar results were obtained, and F5-10 showed the highest capillary water absorption rate, S_1. While for the concrete prepared with shale aggregates, the capillary water absorption rate was related to the aggregate packing volume.

Generally, conventional high-strength lightweight aggregate concrete shows good durability (Chung *et al*. 2021), attributed to the dense ITZ microstructure around lightweight aggregate (Lo *et al*. 1999, Yew *et al*. 2022). Moreover, a preliminary study on the durability of preplaced normal aggregates concrete showed that it had a dense structure and good durability in the marine

environment (Najjar *et al.* 2014). However, F5-10 concrete showed bad durability results that could be attributed to two reasons: on the one hand, a large amount of lightweight aggregates is exposed to the concrete surface, which leads to a rapid increase in capillary water absorption. On the other hand, LWA itself is a porous particle that can contribute to its transport pathways (Bentz and Weiss 2011). The internal lightweight aggregates may connect, establishing diffusion paths for chloride ion diffusion (Bogas *et al.* 2019).

On the other hand, incorporating lightweight aggregates provides a remarkable internal curing effect in cement hydration, improving concrete microstructure (Nie *et al.* 2016, Long *et al.* 2017). However, a large volume of lightweight aggregates with a high water absorption rate may play a negative over-curing effect and increase the porosity of hardened cement paste. Jensen *et al.* (Jensen and Hansen 2001, 2002) proposed the internal curing theory required to obtain the maximum degree of cement hydration. The amount of water introduced could be calculated according to Eqs. (6) and (7)

$$(W/C)_e = 0.18 \cdot (W/C)$$
$$\text{for} \quad W/C \leq 0.36 \tag{6}$$

$$(W/C)_e = 0.42 - (W/C)$$
$$\text{for} \quad 0.36 \leq W/C \leq 0.42 \tag{7}$$

Wherein $(W/C)_e$ is the introduced water-to-cement ratio, and W/C is the effective water-to-cement ratio of the cement paste.

The w/c ratio used in the grouting paste is 0.35, and the required w/c ratio for internal curing could be calculated as 0.063. According to the mix proportions F5-10 and S5-16 in Table 6, the theoretical internal-curing water required for 1m³ F and Y groups is about 33.33 kg and 38.18 kg, respectively. However, the actual water amount introduced by fly ash and shale aggregates is 188.81 kg and 31.83 kg, respectively. Therefore, the water introduced by fly ash aggregates exceeds the required water for complete cement hydration, showing an over-curing effect. Fig. 13 shows the pore size distribution of hardened cement paste around fly ash and shale aggregates. The hardened cement pastes

around fly ash aggregate showed a higher porosity than that around shale aggregate. In addition to the increased refined pores in hardened cement paste around fly ash aggregate, larger pores also increased significantly than around the shale aggregate.

3.3 Effect of asphalt-coated aggregates on PLWAC performance

From Sections 3.1 and 3.2, it could be found that PLWAC with fly ash aggregates showed a higher strength but worse durability. According to previous research, incorporating asphalt-coated ordinary aggregates could improve concrete durability, reducing concrete brittleness, especially for concrete with spherical aggregates (Gao *et al.* 2022). Furthermore, considering the higher brittleness of LWA compared to normal-weight concrete (Dabbaghi *et al.* 2021), incorporating asphalt-coated aggregates is expected to improve concrete toughness simultaneously.

The water absorption rate of fly ash aggregate is very high, different from the ordinary coarse aggregate. Therefore, different soaking times will generate different thicknesses of asphalt film on the surface of the aggregate and different water absorption rates. The mixing water absorption by LWA with different moisture conditions was reflected in the hardened concrete as the variation of its strength (Tang 2017). Fig. 14 shows the effect of the soaking time of the aggregates in asphalt emulsion on the water absorption rate. Compared with the blank group, the water absorption rate of the aggregate soaked for 10 min and 30 min decreased by about 25% and 6%, respectively.

Further increased soaking time to 24 h slightly decreased the water absorption rate to about 4%. Fig. 15 shows the asphalt film thickness as a function of soaking time. When the soaking time increased from 0.5 h to 24 h, the asphalt film thickness on the aggregate surface increased from 42 μm to 120 μm. The thick asphalt film may significantly degrade the ITZ microstructure and decrease the concrete strength and durability (Liu *et al.* 2021). Thus, a soaking time of 30 min was selected for the following experiments.

The effect of asphalt-coated aggregates on concrete durability is shown in Table 9. The chloride diffusion

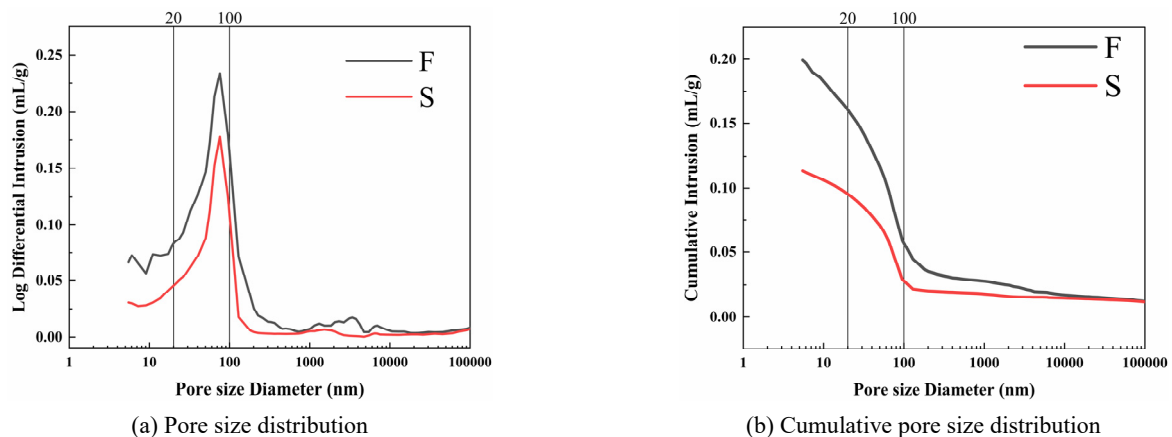(a) Pore size distribution   (b) Cumulative pore size distribution

Fig. 13 MIP analysis of cement pastes around fly ash aggregate (F) and shale aggregate (S)
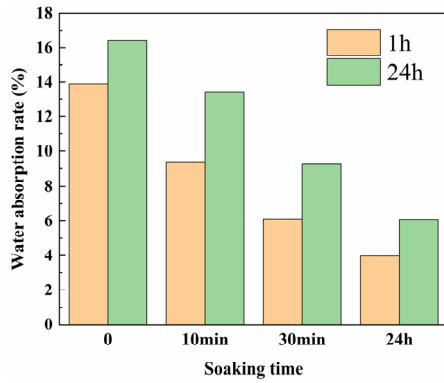
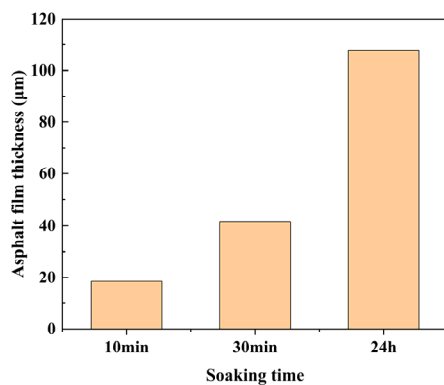Fig. 14 Effect of soaking time on water absorption of aggregates

Fig. 15 Effect of soaking time on the thickness of asphalt film on aggregate surface

Table 9 Effect of asphalt-coated aggregates on the chloride diffusion coefficient

Group	Chloride diffusion coefficient ($\times 10^{-12} m^2/s$)
0	21.85
20-30	10.14
20-100	22.44
40-30	16.76

coefficient of the 20-30 group was reduced by about 53.6 %, which showed the best results. On the one hand, these asphalt-coated aggregates were not pre-saturated, which could absorb water during the mix and curing process. As a result, the internal curing water was reduced from 188.81 kg to about 132.17 kg. On the other hand, concrete durability was also improved due to the introduction of hydrophobic asphalt film (Liu *et al*. 2021). However, the significantly weakened ITZ structure caused by the thick asphalt film may also degrade the concrete durability. That is why the chloride diffusion coefficient of the 20-100 and 40-30 groups slightly changed compared to that of the control group.

Fig. 16 shows the variation of concrete strength incorporating asphalt-coated aggregates. The 20-30 group showed similar strength to the control group. However, the 20-100, 40-30, and 40-100 groups significantly
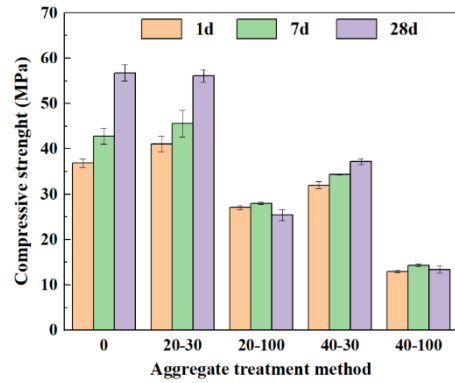

Fig. 16 Effect of asphalt-coated aggregates on the concrete strength

decreased concrete strength, which could also be attributed to the weakened ITZ by incorporating asphalt film.

Figs. 17-18 show the three-point bending-deflection curve and the P-CMOD curves of concretes, respectively. Furthermore, the characteristic parameters of the curve are shown in Table 10. Introducing an appropriate thickness of asphalt film and replacement ratio can improve concrete's peak load and toughness. The coated fly ash aggregate has less water release, decreasing the curing effect. Nevertheless, the cement matrix may be denser because less water content may increase the peak load. Moreover, compared with the blank group, the fracture energy, characteristic length, and peak load of the 20-30 group were
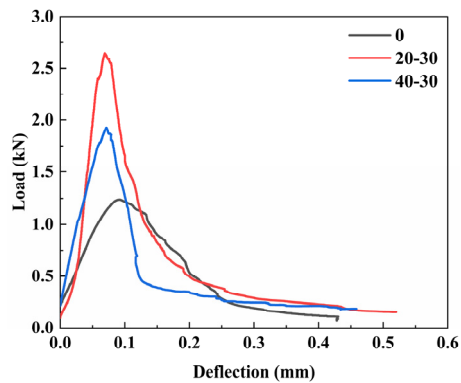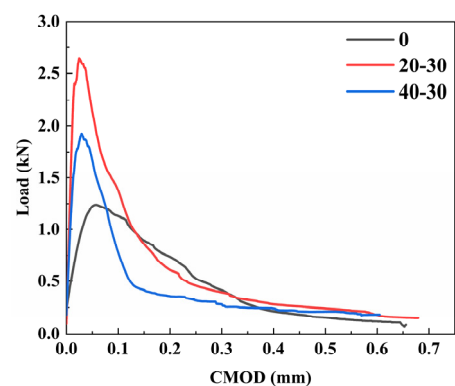

Fig. 17 P-deflection curve of concretes

Fig. 18 P-CMOD curve of concretes

Table 10 Three-point bending test results of concrete prepared with asphalt-coated aggregates

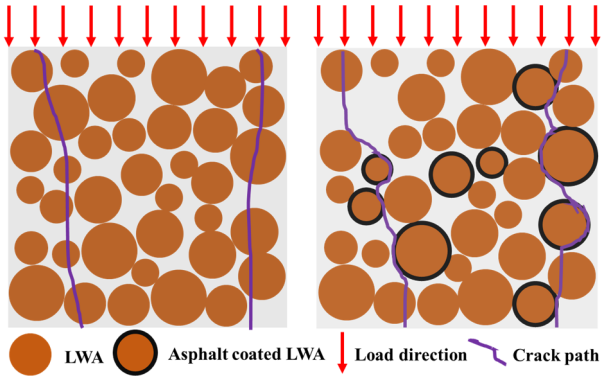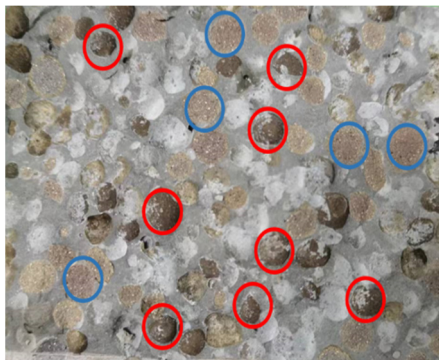| Group	P_{max}/KN		G_f/J·m^{-2}		L_{ch}	
	Mean	SD	Mean	SD	Mean	SD
0	1.24	0.10	38.54	4.22	9.42	1.27
20-30	2.57	0.08	50.23	0.78	19.17	1.28
40-30	2.23	0.30	40.35	0.87	12.68	1.07

Fig. 19 Crack propagation in two concretes
(Left: Conventional LWAC; Right: LWAC prepared with asphalt-coated aggregates)

increased by 30.33%, 103.5%, and 107.26%, respectively. The 40-30 group had a 4.70 % increase in fracture energy, a 34.61% increase in characteristic length, and a 79.84% increase in peak load.

In this study, the improvement in concrete toughness can be first attributed to the fracture-inducing effect of asphalt-coated aggregates. In conventional LWAC, the cracks tend to pass through the aggregates rather than pass around the aggregate due to the low crushing strength of lightweight aggregates and dense ITZ. However, the asphalt-coated lightweight aggregates showed a relatively weak ITZ, which tends to induce crack propagation, as shown in Fig. 19. This would increase the crack propagation path and increase the energy absorbed.

Fig. 20 shows the broken section of 20-30 concrete. As can be seen, most of the broken aggregates were untreated aggregates (blue circle); and the cracks tended to pass around the asphalt-coated aggregates (red circle). While for the ordinary LWAC prepared from fly ash aggregates, almost all the aggregates were fractured due to their relatively low crushing strength.

On the other hand, introducing asphalt film with a high ductility (130 cm @ 15℃) may also increase the absorbed energy. Adding viscoelastic polymer in the ITZ could increase the energy absorbed in the crack's growth, improving concrete toughness Morin *et al.* (2011).

4. Conclusions

The following conclusions could be drawn:

- PLWAC, with compressive strength of 56.8 MPa and a density of 1600 kg/m^3, is prepared using fly ash aggregate with a crush strength of 20 MPa. However, the 1 d and 7 days strength of the concrete with fly ash aggregates and shale aggregates are similar. This may be attributed to gravel shale aggregates' interlocking effect or grouting pastes' ceiling strength.
- The concrete with fly ash aggregates (high crushing strength and high water absorption rate) showed the highest 28 days strength (57.7% higher than concrete prepared with shale aggregates with similar particle grading) while a significant chloride diffusion coefficient (128% higher than concrete prepared with shale aggregates). This is because connected porous fly ash aggregates establish a path for chloride diffusion. Moreover, a negative over-curing effect on the surrounding cement paste may contribute to the increase in the chloride diffusion coefficient.
- By 30% replacement of asphalt pretreated fly ash aggregate with asphalt emulsion (20% solid content), concrete's chloride ion diffusion coefficient can be significantly reduced by 53.5%. In comparison, the peak load increased by 107.3%, and fracture energy by 30.3%. This could be attributed to the over-curing effect reduction and increased absorbed energy during crack propagation.

(a) PLWAC   (b) Ordinary LWAC

Fig. 20 Fractured section of the (a) PLWAC; and (b) ordinary LWAC

Acknowledgments

References

Abdelgader, H.S. and Elgalhud, A.A. (2008), "Effect of grout proportions on strength of two-stage concrete", *Struct. Concrete*, **9**(3), 163-170. https://doi.org/ 10.1680/stco.2008.9.3.163

Al-Azzawi, A.A. and Shallal, M.S. (2021), "Behavior of reinforced sustainable concrete hollow-core slabs", *Adv. Concrete Constr.*, *Int. J.*, **11**(4), 271-294. https://doi.org/10.12989/acc.2021.11.4.271

An, X., Wu, Q., Jin, F., Huang, M., Zhou, H., Chen, C. and Liu, C (2014), "Rock-filled concrete, the new norm of SCC in hydraulic engineering in China", *Cement Concrete Compos.*, **54**, 89-99. https://doi.org/10.1016/j.cemconco mp.2014.08. 001

ASTM (2016), Standard Test Method for Flow of Grout for Preplaced-Aggregate Concrete (Flow Cone Method), ASTM-C939-2016.

Aungatichart, O., Nawaukkaratharnant, N. and Wasanapiarnpong, T. (2022), "The potential use of cold-bonded lightweight aggregate derived from various types of biomass fly ash for preparation of lightweight concrete", *Mater. Lett.*, **327**, 133019. https://doi.org/10/grkn5w

Bentz, D. and Weiss, W. (2011), "Internal Curing: A 2010 State-of-the-Art Review", Report NISTIR – 7765, National Institute of Standards and Technology.

Bogas, J.A., Carriço, A. and Pontes, J. (2019), "Influence of cracking on the capillary absorption and carbonation of structural lightweight aggregate concrete", *Cement Concrete Compos.*, **104**, 103382. https://doi.org/10.1016/j.cemconcomp. 2019.103382

Chia, K.S., Liu, X., Liew, J.Y. and Zhang, M.H. (2014), "Experimental study on creep and shrinkage of high-performance ultra lightweight cement composite of 60 MPa", *Struct. Eng. Mech.*, *Int. J.*, **50**(5), 635-652. https://doi.org/10.12989/sem.2014.50.5.635

Chiou, I.J. and Chen, C.H. (2011), "Properties of artificial lightweight aggregates made from waste sludge", *Comput. Concrete*, *Int. J.*, **8**(6), 617-629. https://doi.org/10.12989/cac.2011.8.6.617

Chung, S.Y., Sikora, P., Kim, D.J., El Madawy, M.E. and Abd Elrahman, M. (2021), "Effect of different expanded aggregates on durability-related characteristics of lightweight aggregate concrete", *Mater. Characteriz.*, **173**, 110907. https://doi.org/10.1016/j.matchar.2021.110907

Coo, M. and Pheeraphan, T. (2016), "Effect of sand, fly ash and limestone powder on preplaced aggregate concrete mechanical properties and reinforced beam shear capacity", *Constr. Build. Mater.*, **120**, 581-592. https://doi.org/10.1016/j.conbuildmat.2016.05.128

Dabbaghi, F., Fallahnejad, H., Nasrollahpour, S., Dehestani, M. and Yousefpour, H. (2021), "Evaluation of fracture energy, toughness, brittleness, and fracture process zone properties for lightweight concrete exposed to high temperatures", *Theor. Appl. Fract. Mech.*, **116**, 103088. https://doi.org/10.1016/j.tafmec.2021.103088

Du, Q., Sun, Q., Lv, J. and Yang, J. (2017), "Use of preplaced

casting method in lightweight aggregate concrete", *Adv. Mater. Sci. Eng.*, 2017. https://doi.org/7234761. 10.1155/2017/7234761

Gao, Y., Liu, P., Wang, F., Hu, C. and Yang, L. (2022), "Organic-inorganic hybrid phyllosilicate with switchable wettability induced by ultrasonication treatment", *Appl. Clay Sci.*, **229**, 106692. https://doi.org/10.1016/j.clay.2022.106692

Haller, T., Beuntner, N., Gutsch, H. and Thienel, K.C. (2023), "Challenges on pumping infra-lightweight concrete based on highly porous aggregates", *J. Build. Eng.*, **65**, 105761. https://doi.org/10.1016/j.jobe.2022.105761

Hillerborg, A., Modéer, M. and Petersson, P.E. (1976), "Analysis of crack formation and crack growth in concrete by means of fracture mechanics and finite elements", *Cement Concrete Res.*, **6**(6), 773-781. https://doi.org/10.1016/0008-8846(76)90007-7

Jensen, O.M. and Hansen, P.F. (2001), "Water-entrained cement-based materials: I. Principles and theoretical background", *Cement Concrete Res.*, **31**(4), 647-654. https://doi.org/10.1016/S0008-8846(01)00463-X

Jensen, O.M. and Hansen, P.F. (2002), "Water-entrained cement-based materials: II. Experimental observations", *Cement Concrete Res.*, **32**(6), 973-978. https://doi.org/10.1016/S0008-8846(02)00737-8

Lilja, S., Maage, M., Simon, P., Aassved, H., Wim, B., Helland, S., Norden, G., Erich, K., Aleksandar, M., Sverre, S., Felipe, T., Ivar, H., Bill, P., Breugel, K. and Thienel, C. (1998), LWAC Material Properties - State-of-the-Art.

Liu, Y., Zhu, Z., Wang, F., Hu, S. and He, Y. (2021), "Effects of asphalt modification of paste–aggregate interface on the transport and mechanical properties of concrete", *J. Mater. Civil Eng.*, **33**(6). https://doi.org/10.1061/(ASCE)MT.1943-5533.0003743

Lo, Y., Gao, X.F. and Jeary, A.P. (1999), "Microstructure of pre-wetted aggregate on lightweight concrete", *Build. Environ.*, **34**(6), 759-764. https://doi.org/10.1016/S0360-1323(98)00060-2

Long, G., Yang, J. and Xie, Y. (2017), "The mechanical characteristics of steam-cured high strength concrete incorporating with lightweight aggregate", *Constr. Build. Mater.*, **136**, 456-464. https://doi.org/10.1016/j.conbuildmat.2016.12.171

Morin, V., Moevus, M., Dubois-Brugger, I. and Gartner, E. (2011), "Effect of polymer modification of the paste–aggregate interface on the mechanical properties of concretes", *Cement Concrete Res.*, **41**(5), 459-466. https://doi.org/10.1016/j.cemconres.2011.01.006

Najjar, M.F., Soliman, A.M. and Nehdi, M.L. (2014), "Critical overview of two-stage concrete: Properties and applications", *Constr. Build. Mater.*, **62**, 47-58. https://doi.org/10.1016/j.conbuildmat.2014.03.021

Nie, S., Hu, S., Wang, F., Yuan, P., Zhu, Y., Ye, J. and Liu, Y. (2016), "Internal curing - A suitable method for improving the performance of heat-cured concrete", *Constr. Build. Mater.*, **122**, 294-301. https://doi.org/10.1016/j.conbuildmat.2016.05.159

Nie, S., Zhang, W., Hu, S., Liu, Z. and Wang, F. (2018), "Improving the fluid transport properties of heat-cured concrete by internal curing", *Constr. Build. Mater.*, **168**, 522-531. https://doi.org/10.1016/j.conbuildmat.2018.02.068

Real, S., Bogas, J.A. and Pontes, J. (2021), "Structural lightweight aggregate concrete exposed to marine environment for 5 years", *Constr. Build. Mater.*, **275**, 122161. https://doi.org/10.1016/j.conbuildmat.2020.122161

Revilla-Cuesta, V., Fiol, F., Perumal, P., Ortega-López, V. and Manso, J.M. (2022), "Using recycled aggregate concrete at a precast-concrete plant: A multi-criteria company-oriented feasibility study", *J. Cleaner Prod.*, **373**, 133873. https://doi.org/10.1016/j.jclepro.2022.133873

Rustamov, S., Kim, S., Kwon, M. and Kim, J. (2021), "Effects of

fiber types and volume fraction on strength of lightweight concrete containing expanded clay", *Adv. Concrete Constr., Int. J.*, **12**(1), 47-55. https://doi.org/10.12989/acc.2021.12.1.047

Shoaei, P., Zolfaghary, S., Jafari, N., Dehestani, M. and Hejazi, M. (2017), "Investigation of adding cement kiln dust (CKD) in ordinary and lightweight concrete", *Adv. Concrete Constr., Int. J.*, **5**(2), 101-115. https://doi.org/10.12989/acc.2017.5.2.101

Siddique, S., Kim, H., Son, H. and Jang, J.G. (2021), "Characteristics of preplaced aggregate concrete fabricated with alkali-activated slag/fly ash cements", *Materials*, **14**(3). https://doi.org/10.3390/ma14030591

Tang, C.-W. (2017), "Effect of presoaking degree of lightweight aggregate on the properties of lightweight aggregate concrete", *Comput. Concrete, Int. J.*, **19**(1), 69-78. https://doi.org/10.12989/cac.2017.19.1.069

Vakhshouri, B. and Nejadi, S. (2017), "Compressive strength and mixture proportions of self-compacting light weight concrete", *Comput. Concrete, Int. J.*, **19**(5), 555-566. https://doi.org/10.12989/cac.2017.19.5.555

Vali, K.S. and Murugan, S.B. (2020), "Effect of different binders on cold-bonded artificial lightweight aggregate properties", *Adv. Concrete Constr., Int. J.*, **9**(2), 183-193. https://doi.org/10.12989/acc.2020.9.2.183

Yang, Y., Chen, Y., Yang, Y. and Zeng, S. (2019), "Investigation on mechanical performance of flat steel plate-lightweight aggregate concrete hollow composite slab", *Steel Compos. Struct., Int. J.*, **31**(4), 329-340. https://doi.org/10.12989/scs.2019.31.4.329

Yew, M.K., Beh, J.H., Yew, M.C., Lee, F.W., Saw, L.H. and Lim, S.K. (2022), "Performance of surface modification on bio-based aggregate for high strength lightweight concrete", *Case Stud. Constr. Mater.*, **16**, e00910. https://doi.org/10.1016/j.cscm.2022.e00910

Yoon, J.Y. and Kim, J.H. (2019), "Mechanical properties of preplaced lightweight aggregates concrete", *Constr. Build. Mater.*, **216**, 440-449. https://doi.org/10.1016/j.conbuildmat.2019.05.010

Yoon, J.Y., Kim, J.H., Hwang, Y.Y. and Shin, D.K. (2015), "Lightweight concrete produced using a two-stage casting process", *Mater.*, **8**(4), 1384-1397. https://doi.org/10.3390/ma8041384

Yoon, J.Y., Lee, J.Y. and Kim, J.H. (2019), "Use of raw-state bottom ash for aggregates in construction materials", *J. Mater. Cycl. Waste Manage.*, **21**(4), 838-849. https://doi.org/10.1007/s10163-019-00841-5

Yoon, J., Kim, H., Shin, S.W. and Sim, S.H. (2020), "Rheology-based determination of injectable grout fluidity for preplaced aggregate concrete using ultrasonic tomography", *Constr. Build. Mater.*, **260**, 120447. https://doi.org/10.1016/j.conbuildmat.2020.120447

JK